Self and mutual capacitance of conductors in air and lossy earth with application to electrified railways

Andrea Mariscotti

ARCHIVES OF ELECTRICAL ENGINEERING VOL. 68(4), pp. 859–873 (2019)

DOI 10.24425/aee.2019.130688

Self and mutual capacitance of conductors in air and lossy earth with application to electrified railways

ANDREA MARISCOTTI

University of Genoa
Italy
e-mail: andrea.mariscotti@gmail.com

(Received: 04.05.2019, revised: 01.07.2019)

Abstract: The problem of a closed-form accurate determination of self and mutual capacitance of conductors in air and earth is considered: the application is the complete modeling of a railway line including buried conductors. The Generalized Potential Method (GPM) is presented and analyzed with regard to conditions of validity and solution methods. The accuracy of the GPM is evaluated solving some reference cases using the Complex Image Method and a commercial Finite Element Method simulator, comparing the model results with experimental data, and including the sensitivity on soil conductivity and permittivity, distance of conductors from the air–earth interface and frequency.

Key words: capacitance, electromagnetic coupling, electrified rail systems, electromagnetic modeling

1. Introduction

The increasing complexity of electrified railways, with new signalling systems on one side [1–3] and a wider utilization of power electronic converters (a source of disturbance above the usual power system harmonics [4–6]) make necessary including the variability of electric parameters in simulation models.

Various methods have appeared in the literature: Multiconductor Transmission Line (MTL) models [7] were used for both frequency- and time-domain analysis of electric networks [8–10] and interference to signaling and telecommunications [2, 3]. These methods rely on accurate parameters values (including influence of frequency), as for running rails [11–16] and coupling between line conductors, with capacitive terms in general less accurate than inductive ones

[17, 18]. In this work self and mutual capacitance terms are evaluated with a closed-form direct approach with good accuracy for conductors in the air, inside the earth or at the air–earth interface, the frequency ranging up to some tens of kHz [1, 2].

The Complex Image Method (CIM) [19, 20] is the simplest method, but valid only in the air region with a conductive earth (see section 2). The Generalized Potential Method (GPM) [19] is based on the potential coefficients and will be developed and discussed in section 3, and evaluated in section 5 against a Finite Element Method (FEM) simulator and CIM with a range of earth conductivity σ_e and dielectric permittivity ε_e values.

FEM methods are quite diffused and applicable to arbitrary geometries [21]; however, application in the railway domain is often limited to low frequency (e.g. stray current or magnetic field at power frequency) and small domains, such as running rails [11–22].

Self and mutual capacitance coefficients for a generic conductor system are defined in terms of charge $\boldsymbol{Q}$ and potential $\boldsymbol{V}$ [20, 23], related by the "capacitance coefficient matrix" $\boldsymbol{c}$.

$$\begin{cases} Q_1 = c_{11}V_1 + c_{12}V_2 + \ldots + c_{1n}V_n \\ Q_2 = c_{21}V_1 + c_{22}V_2 + \ldots + c_{2n}V_n \\ \vdots \\ Q_n = c_{n1}V_1 + c_{n2}V_2 + \ldots + c_{nn}V_n \end{cases} . \tag{1}$$

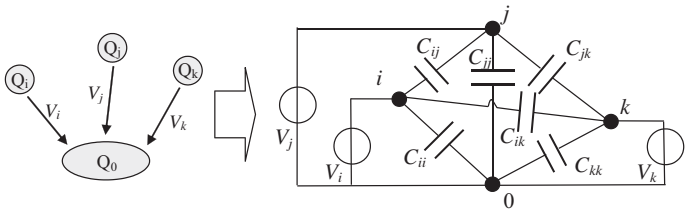

Fig. 1. Real conductors in lossy medium and equivalent circuit for capacitance calculation

Under quasi-stationary assumption, with conductor 0 as reference, (1) may be written as in (2), with $V_i - V_j$ the difference of potential between conductors i and j.

$$\begin{cases} Q_1 = C_{10}V_1 + C_{12}(V_1 - V_2) + \ldots + C_{1n}(V_1 - V_n) \\ Q_2 = C_{21}(V_2 - V_1) + C_{20}V_2 + \ldots + C_{2n}(V_2 - V_n) \\ \vdots \\ Q_n = C_{n1}(V_n - V_1) + C_{n2}(V_n - V_2) + \ldots + C_{n0}V_n \end{cases} . \tag{2}$$

The new capacitance matrix is called "generalized capacitance matrix" $\boldsymbol{C}$. The relationship between the terms c_{ij} of $\boldsymbol{c}$ and the terms C_{ij} of $\boldsymbol{C}$ is

$$C_{i0} = c_{ii} + \sum_{j=1,\ j\neq i}^{n} c_{ij}\,, \qquad C_{ik} = -c_{\underset{i\neq k}{ik}}\,. \tag{3}$$

2. Complex image method

The Complex Image Method (CIM) [19, 20] may be applied if, first, conductors length is larger than a system cross section, and, second, the earth behaves as a perfect conductor, used as a symmetry plane. Then, symmetric fictitious conductors in the earth region can be assumed, so that the earth is replaced by an equipotential surface (see Fig. 2). The problem is thus reduced to the computation of mutual capacitance: the self term is calculated for conductor i and its underground image i'; the mutual term considers conductors i and j and i and j'.

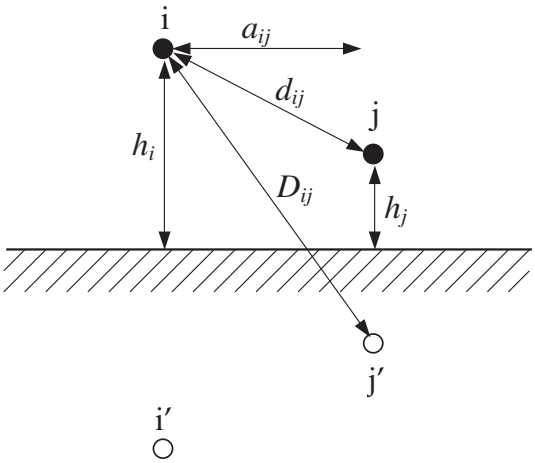

Fig. 2. CIM geometry

The capacitance terms are determined by calculating the coefficients of potential:

$$w_{ii} = \frac{1}{2\pi\varepsilon_0} \ln\left(2h_i/r_i\right), \qquad w_{ij} = w_{ji} = \frac{1}{2\pi\varepsilon_0} \ln\left(D_{ij}/d_{ij}\right), \tag{4}$$

$$C_{ii} = (w_{ii})^{-1}, \qquad C_{ij} = \frac{w_{ij}}{w_{ii} \cdot w_{jj}}. \tag{5}$$

3. Generalized potential method

This method is based on Maxwell's equations for a cylindrical geometry [19]: magnetic and electric fields have exponential dependency on the longitudinal z-axis (see Fig. 3) with the propagation constant γ.

$$\begin{aligned} \vec{E}(x, y, z) &= \vec{E}(x, y) \cdot e^{-\gamma z}, \\ \vec{H}(x, y, z) &= \vec{H}(x, y) \cdot e^{-\gamma z}. \end{aligned} \tag{6}$$

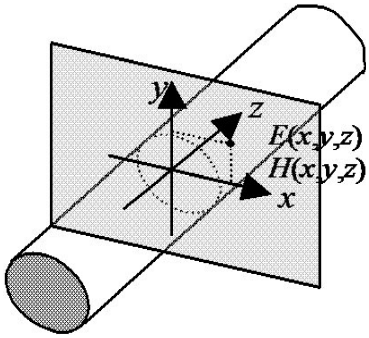

Fig. 3. Sketch of the electric and magnetic field vectors along a conductor

The transversal components of the magnetic and electric field are then

$$\begin{aligned} E_x &= -\frac{1}{k^2+\gamma^2}\cdot\left(j\omega\mu\frac{\partial H_z}{\partial y}+\gamma\frac{\partial E_z}{\partial x}\right),\\ E_y &= \frac{1}{k^2+\gamma^2}\cdot\left(j\omega\mu\frac{\partial H_z}{\partial x}-\gamma\frac{\partial E_z}{\partial y}\right),\\ H_x &= \frac{1}{k^2+\gamma^2}\cdot\left(j\omega\bar{\varepsilon}\frac{\partial E_z}{\partial y}-\gamma\frac{\partial H_z}{\partial x}\right),\\ H_y &= \frac{1}{k^2+\gamma^2}\cdot\left(j\omega\bar{\varepsilon}\frac{\partial E_z}{\partial x}+\gamma\frac{\partial H_z}{\partial y}\right). \end{aligned} \tag{7}$$

$$\bar{\varepsilon} = \varepsilon + \frac{\sigma}{j\omega}, \ldots k^2 = \omega^2\mu\bar{\varepsilon}\,. \tag{8}$$

Boundary conditions are then specified to ensure continuity of magnetic and electric field components at each layer interface (m, m+1), considering a generic multi-layer system:

$$\begin{aligned} &E_{m,x}(x,y,z) = E_{m+1,x}(x,y,z), \qquad E_{m,y}(x,y,z) = E_{m+1,y}(x,y,z),\\ &H_{m,x}(x,y,z) = H_{m+1,x}(x,y,z), \qquad H_{m,y}(x,y,z) = H_{m+1,y}(x,y,z). \end{aligned} \tag{9}$$

The propagation constant γ is determined by solving one additional boundary condition on the continuity of the longitudinal electric field at the interface between the conductor and the layer (either air or soil) that surrounds it:

$$E_z = Z_i^{e/e} + j\omega L_{ci} - \gamma^2 w_{ci}\,, \tag{10}$$

where L_{ci} and w_{ci} refer to the conductor coating (zero for bare conductors); $Z_i^{e/e}$ is the external return surface impedance of conductor i and for a solid conductor is:

$$Z_i^{e/e} = \frac{\rho_i\chi_i}{2\pi r_i}\cdot\frac{I_0(\chi_i r_i)}{I_1(\chi_i r_i)}, \qquad \chi_i = \sqrt{-k_i^2-\gamma^2}. \tag{11}$$

I_0 and I_1 are the modified Bessel functions of the first kind of zero and first order.

The electric field solution for any layer, for a given excitation current I, may be written as

$$E_z = f \cdot I + \gamma^2 g \cdot I, \tag{12}$$

where f is related to the inductive part and g to the scalar potential (notation as in [19]):

$$V = \gamma\, g \cdot I. \tag{13}$$

The expressions for the scalar potential of a conductor in the air or in the earth are given in (14) and (15), respectively, where (x_1, y_1) and (x_2, y_2) represent a point in the two regions:

$$V_1 = \frac{\gamma I e^{-\gamma z}}{j\omega 2\pi \overline{\varepsilon}_1}\left[K_0\left(\chi_1 R\right) - K_1\left(\chi_1 R'\right) + \int_{-\infty}^{+\infty} \frac{k_1^2 e^{-u_1(x_1+h_1)} e^{-j\lambda(y_1-d_1)}}{k_1^2 u_2 + k_2^2 u_1}\,\mathrm{d}\lambda\right], \tag{14}$$

$$V_2 = \frac{\gamma I e^{-\gamma z}}{j\omega 2\pi \overline{\varepsilon}_2}\left[K_0\left(\chi_2 R\right) - K_1\left(\chi_2 R'\right) + \int_{-\infty}^{+\infty} \frac{k_2^2 e^{u_2(x_2+h_2)} e^{-j\lambda(y_2-d_2)}}{k_1^2 u_2 + k_2^2 u_1}\,\mathrm{d}\lambda\right]. \tag{15}$$

K_0 and K_1 are modified Bessel functions of the second kind of zero and first order. The two first leftmost terms correspond to the CIM, but the rightmost integrals may be interpreted as "corrective terms": k_i and $\overline{\varepsilon}_i$ terms are defined in (8), identified by indexes 1 and 2 for each of the two regions, air or earth.

The propagation constant γ is determined with the constraint of the continuity of the tangential electric field at each medium-conductor interface (eq. (4) in [23]). Calculations developed in [23] lead to the following eigenvalue equation (eq. (12) in [23], where a typing mistake was found: the k_0 exponent is +2 and not −2).

$$\left|\gamma^2 \boldsymbol{U} - k_0^2 \boldsymbol{A}\right| = 0. \tag{16}$$

The solution of (16) for both regions must be made numerically, by minimization of the objective function taken as the square of (16); a troublesome sensitivity to the starting point was found, that require some care. Simplified expressions for γ [19, 23] are

$$\gamma \cong jk = j\sqrt{j\omega\mu(\sigma + j\omega\varepsilon)}, \tag{17a}$$

$$\gamma \cong jk = j\sqrt{j\omega\mu(j\omega\varepsilon)}, \tag{17b}$$

where (17a) is for the large conductivity region (the earth) and (17b) is for the air region. The effect of these two expressions on self and mutual capacitance is evaluated in section 5.

The evaluation of the integral term in (14) and (15) is critical due to the shape of the integrand: very steep for small λ and going to 0 very slowly for increasing λ, so that a logarithmic distribution of λ was chosen sufficiently accurate near the origin and extended for several orders of magnitude with economy of points.

The two quantities R and R' given in (18) indicate the distance between a generic point (x, y) at a fixed longitudinal section z and a reference conductor, placed at d_i, h_i coordinates.

$$R = \sqrt{(x - h_i)^2 + (y - d_i)^2}, \qquad R' = \sqrt{(x + h_i)^2 + (y - d_i)^2}. \tag{18}$$

The coefficients of potential w_{ij} can be calculated by relating the scalar potential V to the transversal current I^t, corresponding to the inverse of the coefficients of admittance y_{ik}.

$$w_{ij} = \frac{V}{I^t} = \gamma g, \qquad y_{ij} = w_{ij}^{-1} . \tag{19}$$

Under the assumption of exponential dependency on the z-axis the transversal current is

$$I^t = Ie^{-\gamma z}. \tag{20}$$

From the coefficients of admittance, conductance and capacitance terms are derived as

$$y_{ij} = g_{ij} + j\omega \cdot c_{ij} . \tag{21}$$

These expressions are valid for systems which may be described with a cylindrical geometry; they take into account the soil conductivity and permittivity and can be applied to conductors in the air and in the earth.

4. Permittivity and conductivity of soil

Reference intervals for the permittivity ε_e and conductivity σ_e of earth can be derived from experimental data, for different types of soil [24, 34]. Some of these data were measured at UHF or higher frequency [24, 34]. The relative permittivity of pure dried solid materials [24] ranges up to about 10 (about 20–40, in one case in the presence of unavoidable small % of water). If water and wet materials are included, then values up to the 80 of pure water may be found [25]. Authors of [24] and [25] agree that montmorillonite mineral may reach high values (up to 210 [25, 26]). Deep absorption of water accounts for fluid-rock electrochemical interaction and increases permittivity [25]. Soil conductivity shows a larger range of values: usual values are between 0.01 and 100 mS/m, for various geological types and environmental conditions. In [27] resistivity varies between a few Ωm up to about 50 kΩm for water content ranging from 100% down to 0.1%; similarly permittivity varies from 100 000 down to 100 (same water %) at 10 Hz and reduces to 1 000–10 at 100 kHz. These values are quite large and unusual, and not confirmed by other sources. Longley-Rice soil characteristics [30] show 4–25 permittivity and 1–20 mS/m conductivity intervals for "poor", "average" and "good" ground.

In general, depending on the yearly cyclic water content and temperature, resistivity changes about by a factor of 4 [33]. In [35] it is observed that the dependency of resistivity on temperature is weak between 25 and 0°C, but below resistivity tends to increase more rapidly.

The permittivity ε_r for imperfect dielectrics is a complex quantity, with a real part ε_r' (associated with energy storage and dipole orientation) and an imaginary part ε_r'' (made of relaxation losses and $\sigma_{dc}/(2\pi f\varepsilon_0)$, with σ_{dc} ionic conductivity, that may play a role at low frequency) [8]. The used permittivity term for ε_e is thus associated with the real part of ε_r.

Relevant information for various mineral and soil types is shown in Table 1.

Table 1. Relative permittivity and conductivity of soil and minerals

Mineral/Soil	**Data source and values**			
	Relative permittivity		**Conductivity [mS/m]**	
Quartz	4.2–4.5 @ ≥ 1 MHz (O, V)		1.3×10^{-15} [34] (fused)	$(5–25000) \times 10^{-12}$ [34]
Calcite	7.8–9.1 @ ≥ 1 MHz (O, V, K)		10^{-10} [34]	
Kaolin	11.8 @ 1 MHz (O); 5.2 @ ≥ 2.5 MHz (F)		n.a.	n.a.
Montmorillonite	207–210 @ 1 MHz (O); 10.4 @ 2.5 MHz (F); 5.5 @ ≥ 100 MHz [24, 25]		n.a.	n.a.
Granite	4–6 (DA)	5–7 (D)	1 [33]	
Sand (dry/wet)	3–5/20–30 (DA)	4–6/10–30 (D)	2 [27] 0.5–50 [33]	0.05–0.2 [27] (arid sand)
Clay (dry/wet)	2–6/15–40 (D)		4 [27]	10/500 [33]
Soil (dry/wet)	4–6/10–30 (D)		8–12 [27] (rich soil, lawns, marshes)	0.1–0.5 dry 10–30 wet [28]
Limestone	4–8 (DA, D)		0.1–200 [33]	

Notes: {F: Ficai, 1959; O: Olhoeft, 1989; V: von Hippel, 1954; K: Keller, 1989} in [24];
{DA: Davis and Annan, 1989; D: Daniels, 1996; K: Keller, 1989; O: Olhoeft, 1981} in [25].

5. Validation and results

The assessment of the accuracy of approximate expressions (17a) and (17b) of γ for self and mutual capacitance terms above 10 Hz gives a maximum error in air and earth of 10% and 25% for a conductor position of ±5 m: they will be used in the rest of the paper. A GPM is validated against a CIM (for air region) and the Maxwell FEM [36]. The problem in Fig. 4 has two conductors of 6 mm radius, with conductor 1 at h_1 height and the other moving.

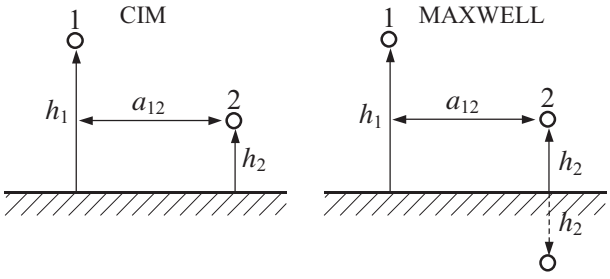

Fig. 4. Geometries for GPM validation with CIM (left) and Maxwell (right)

5.1. Validation of GPM implementation with CIM (air-air)

In Fig. 5 the self C_{ii} and mutual C_{ij} capacitance are shown for two conductors in the air, one fixed ($h_1 = 0.5$ m) and one at variable height $h_2 > 0$, displaced horizontally with $a_{12} = 0.5$ m.

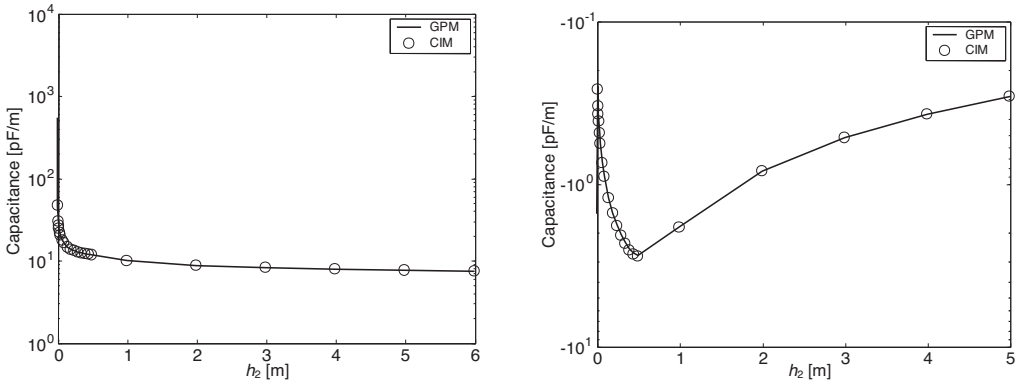

Fig. 5. (a) self-capacitance and (b) mutual capacitance vs. h_2 (conductors in air)

The air is a perfect dielectric and the results of the CIM and GPM overlap. The self-term in Fig. 5a decreases with increasing h_2, while the mutual term in Fig. 5b exhibits a maximum value (y-axis values are negative) for minimum separation between conductors ($h_1 = h_2$).

The self and mutual capacitance show a step change when conductor 2 leaves the earth region and goes into the air region. As a confirmation, if conductivity σ and electric permittivity ε are the same for the two regions, then the step change disappears (see Fig. 6). The residual small "hill" is due to the influence of the other conductor in $h_2 = 0.5$ m (the top of this hill is not

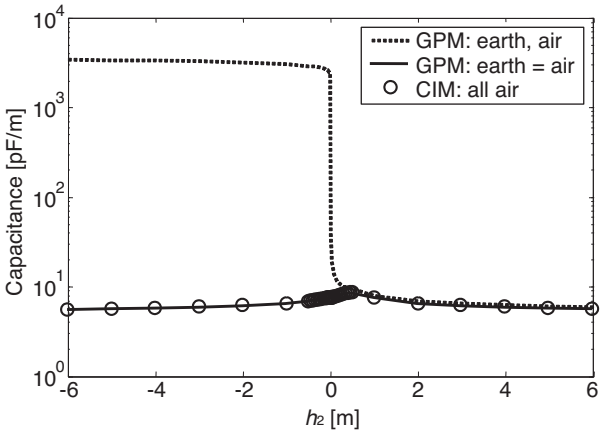

Fig. 6. Mutual cap. vs. height (identical ε_e and σ_e values for the two regions, earth and air)

centered above 0, but shifted to the right); these GPM values are confirmed by a CIM test in which the conductors are placed in air with the earth plane pushed far away.

In practice the division between the air and earth region is not usually sharp and precise, so there will be a "gray zone" (where the conductor is neither completely buried nor surrounded by air, as it is for running rails), for which either of the two methods apply exactly.

5.2. Validation with Maxwell® (air–earth and earth–earth scenarios)

For configurations where at least one conductor is in the earth region, a GPM is validated with a FEM program, Maxwell® Student Version [36]. Results of the GPM and Maxwell are shown in Fig. 7 for two values of $\varepsilon_e (= 1\,000)$ and $\sigma_e (= 10$ mS/m) in the air–earth problem.

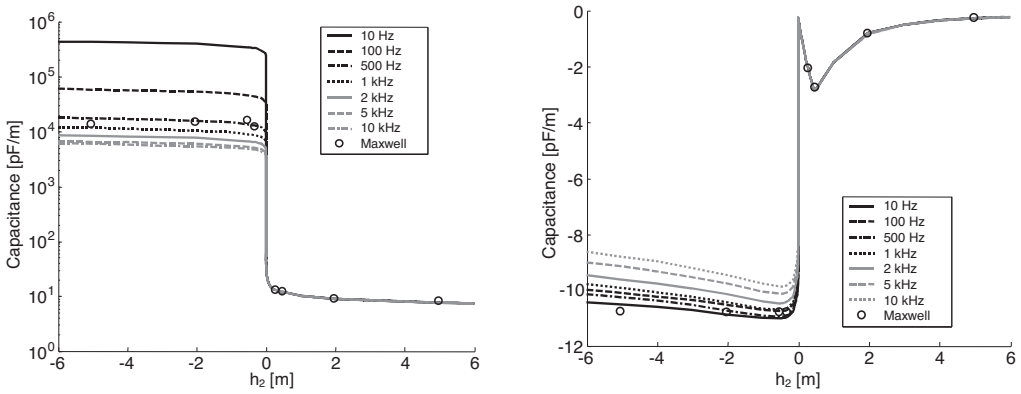

Fig. 7. (a) self and (b) mutual capacitance vs. frequency with $\varepsilon_e = 1\,000$ and $\sigma_e = 10$ mS/m (GPM lines and Maxwell circles) (air–earth)

When $h_2 > 0$ the GPM and Maxwell results are almost identical, whereas for $h_2 < 0$ the GPM shows significant frequency dependency, overlapping the FEM values. The self term features two orders of magnitude of variation for a three decade increase of frequency (in agreement with the expected sqrt(f) dependency for skin depth in earth [8]), while the mutual term is much less variable, as the series of air and earth terms. The agreement is also confirmed with the results shown in [14], Tables 6 and 7, and [16], Fig. 7, for differential track measurements, having combined self and mutual terms; [13], Fig. 25, shows a smaller change of only one order of magnitude for the same three decades of frequency. Focusing on the air–earth interface, a quantitative comparison is undergone: in [13], Fig. 43, the self-term values at 100 Hz and 1 kHz are about 90 and 30 nF/m, well matching the dashed curve of Fig. 7(a) at 63 and 18 nF/m. The values in [14], Table 7, are those of a differential two-port circuit, i.e. rail-to-rail capacitance, equal to 1/2 of the self-capacitance, assuming a negligible mutual capacitance; in this case at 100 Hz the 2×34.3 nF/m value is in agreement with the calculated 63 nF/m value.

The analysis is completed with the solution of the earth–earth problem, where conductor 1 of Fig. 4 is placed in the earth with depth $h_1 = 0.5$ m.

The dependency of self-capacitance on earth permittivity ε_e is negligible at very low frequency (Table 2, 10 Hz row), increasing at higher frequency (Table 2, 100 Hz and 1 kHz). The influence of earth conductivity σ_e value is nearly proportional to the frequency (Table 3).

Table 2. Self-capacitance in earth vs. frequency and permittivity

$h_2 = -2$ m	Self-capacitance [F/m] with $\sigma_e = 10^{-3}$ S/m		
	$\varepsilon_e = 10$	$\varepsilon_e = 100$	$\varepsilon_e = 1\,000$
10 Hz	3.770×10^{-7}	3.773×10^{-7}	3.799×10^{-7}
100 Hz	4.821×10^{-8}	4.850×10^{-8}	5.140×10^{-8}
1 kHz	6.401×10^{-9}	6.737×10^{-9}	1.009×10^{-8}

Table 3. Self-capacitance in earth vs. frequency and conductivity

$h_2 = -2$ m	Self-capacitance [F/m] with $\varepsilon_e = 100$		
	$\sigma_e = 10^{-1}$ S/m	$\sigma_e = 10^{-3}$ S/m	$\sigma_e = 10^{-4}$ S/m
10 Hz	6.351×10^{-5}	3.798×10^{-7}	6.665×10^{-9}
100 Hz	8.828×10^{-6}	5.140×10^{-8}	2.826×10^{-9}
1 kHz	1.326×10^{-6}	6.738×10^{-9}	3.333×10^{-10}

Considering Tables 2 and 3 (neglecting the smaller mutual capacitance), the average change from 10 to 100 Hz (7.5), and 100 Hz to 1 kHz (7.2) for the most common values of ε_e and σ_e, is in good correspondence with the results in [15], less than 9 and larger than 6, respectively.

The mutual capacitance has a more complex behavior being the combination of air and earth region terms: Fig. 8 shows good agreement with Maxwell results. A peculiar aspect may be highlighted: for each ε_e there is a σ_e value for which the corrective terms of (18) and (18) start to diverge at large distance, the larger σ_e the smaller the distance value.

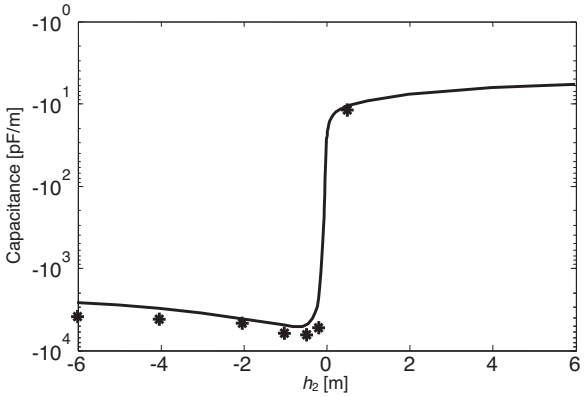

Fig. 8. Mutual capacitance vs. h_2 with $\varepsilon_e = 1\,000$ and $\sigma_e = 10^{-5}$ S/m (∗ Maxwell) (earth–earth)

5.3. Sensitivity analysis

The dependency of self and mutual capacitance on soil permittivity ε_e and conductivity σ_e is analyzed observing that small values of σ_e can change the earth behavior from an imperfect dielectric to an imperfect conductor. Results are shown in Fig. 9 for ε_e and in Fig. 10 for σ_e.

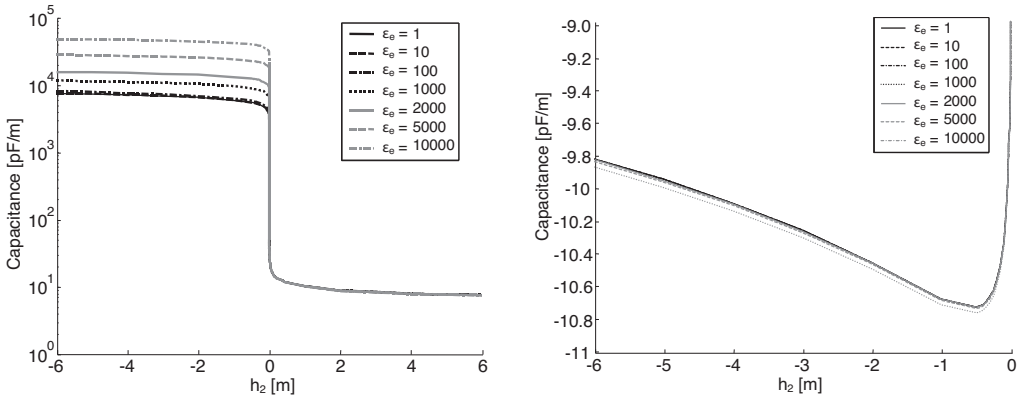

Fig. 9. (a) self and (b) mutual capacitance vs. h_2 with rel. $\varepsilon_e = 1 \div 10^4$ and $\sigma_e = 0.01$ S/m (air–earth)

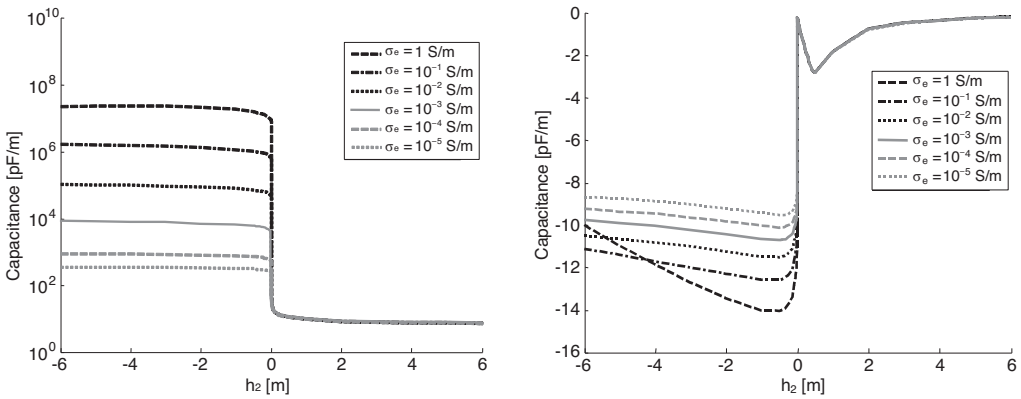

Fig. 10. (a) self and (b) mutual capacitance vs. h_2 with $\sigma_e = 10^{-5} \div 1$ S/m and rel. $\varepsilon_e = 100$ (air–earth)

The largest value (1 S/m) is extreme and uncommon: it appears for completeness and significantly affects the slope of the mutual term in Fig. 10(b); also the smallest value 10^{-5} S/m is quite uncommon, but it is not an issue for calculations.

Fig. 11 shows the buried conductor at a depth $h_2 = 2$ m with a frequency of 1 kHz. For common ε_e values self and mutual capacitance are almost constant (in agreement with the common assumption that they are "geometric parameters" for an ideal dielectric). The dependency on σ_e

is nearly linear; for large σ_e values the problem is no longer electrostatic, since the earth becomes an imperfect conductor. The mutual terms are almost independent on earth parameters thanks to the predominance of the air region.

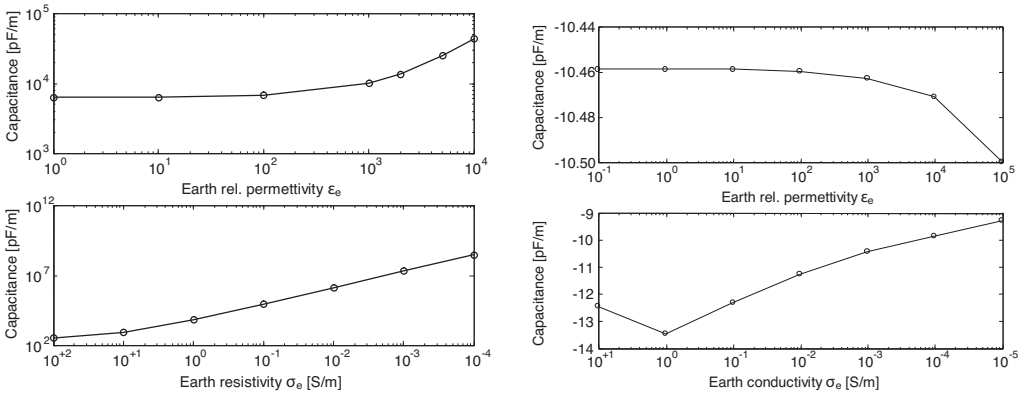

(a) (b)

Fig. 11. (a) self and (b) mutual capacitance with $h_2 = 2$ m and $f = 1$ kHz vs. ε_e and ρ_e (air–earth)

For the earth–earth problem the dependency of the mutual capacitance on σ_e for given ε_e and f is considered (Fig. 12). Tested values are extreme in that there are combinations of ε_e, σ_e and f for which the integrals diverge and the resulting mutual capacitance is positive.

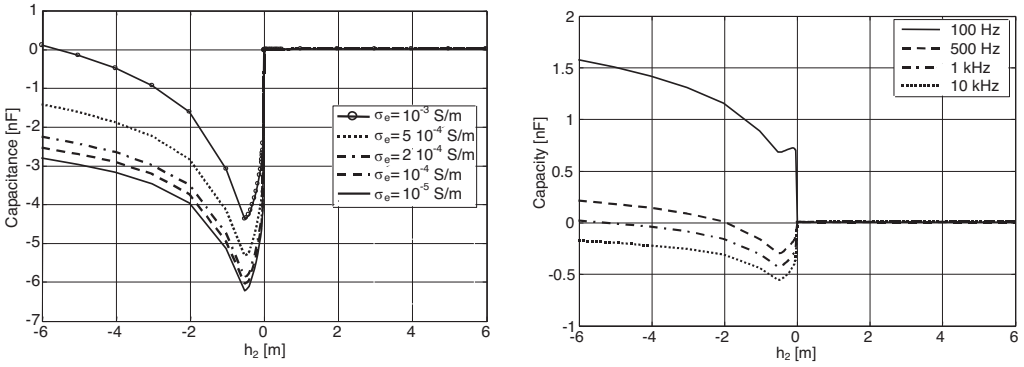

(a) (b)

Fig. 12. (a) self and (b) mutual capacitance vs. h_2 and $f = 0.1, \ldots, 10$ kHz with $\sigma_e = 10^{-3}$ S/m and rel. $\varepsilon_e = 1\,000$ (earth–earth)

In general, we may say that the corrective terms (18) are needed to extend CIM terms to the earth region (the air–earth mutual capacitance terms would be otherwise zero); the phenomenon occurs when the amplitude of the imaginary part of the complex dielectric constant (10) is larger than the real part.

Verification of equations in [19] has shown that closed-form expressions and related results are generally derived under a low frequency assumption, so that the highlighted phenomenon is not evident, but applicability to higher frequency is thus not ensured.

6. Conclusions

A set of expressions for the closed form calculation of a self and mutual capacitance term for conductors in air and earth is presented. The validity of expressions is checked against simple calculations for conductors in the air region and Finite Element Method simulations for the inclusion of the earth region. The results are, in general, very good with the exception of a set of earth electrical properties and frequency values for which the integral corrective terms for mutual capacitance terms diverge. A cross check of the phenomenon against the expressions reported in [19] was not possible, since expressions there are developed and solved under the simplifying "low frequency" assumption, that does not suffer divergence problems, but cannot accurately model behavior at even moderately high frequency.

Experimental results of track capacitance published in the literature have been used to confirm the calculated values in some conditions (geometry, frequency, soil resistivity and permittivity), although the studied method is in general applicable to conductors within the earth, being non-cylindrical conductors at the air–earth interface quite a difficult benchmark.

The proposed formulation is thus useful to complement static or low frequency formulations, including the effect of soil also for increasing frequency, limited by the behavior of the complex permittivity and divergence of integrals.

References

[1] CENELEC Std. CLC/TS 50238-2, *Railway applications – Compatibility between rolling stock and train detection systems – Part 2: Compatibility with track circuits* (2010).

[2] Mariscotti A., Ruscelli M., Vanti M., *Modeling of audiofrequency track circuits for validation, tuning and conducted interference prediction*, IEEE Trans. on Intelligent Transportation Systems, vol. 11, no. 1, pp. 52–60 (2010).

[3] Yuan L., Yang Y., Hernández A., Shi L., *Novel adaptive peak detection method for track circuits based on encoded transmissions*, IEEE Sensors Journal, vol. 18, no. 15, pp. 6224–6234 (2018).

[4] Steimel A., *Electric traction – Motive power and Energy supply: basic and practical experience*, Oldenbourg Industrieverlag, Munich, Germany (2008).

[5] Steczek M., Chudzik P., Szeląg A., *Combination of SHE and SHM – PWM techniques for VSI DC-link current harmonics control in railway applications*, IEEE Trans. on Industrial Electronics, vol. 64, no. 10, pp. 7666–7678 (2017).

[6] Yang Z., Li H., Feng C., Jiang Y., Lin F., Yang Z., *Survey on electromagnetic interference analysis for traction converters in railway vehicles*, Proceedings of the International Power Electronics Conference (2018), DOI: 10.23919/IPEC.2018.8507954.

[7] Paul C., *Multiconductor Transmission Lines*, J. Wiley, New York (1991).

[8] Mariscotti A., Pozzobon P., *Determination of the electrical parameters of railway traction lines: calculation, measurement and reference Data*, IEEE Trans. on Power Delivery, vol. 19, no. 4, pp. 1538–1546 (2004).

[9] Hemmer B., Mariscotti A., Wuergler D., *Recommendations for the calculation of the total disturbing return current from electric traction vehicles*, IEEE Trans. on Power Delivery, vol. 19, no. 2, pp. 1190–1197 (2004).

[10] Dolara A., Leva S., *Multiconductor transmission line models for PQ and EMC analysis of railway electrification systems*, International Review of Electrical Engineering, vol. 7, no. 5, pp. 5795–5807 (2012).

[11] Hill R.J., Carpenter D.C., *Rail track distributed transmission line impedance and admittance: theoretical modeling and experimental results*, IEEE Trans. on Vehicular Technology, vol. 42, no. 2, pp. 225–241 (1993).

[12] Szeląg A., *Rail track as a lossy transmission line. Part I: Parameters and new measurement methods*, Archives of Electrical Engineering, vol. 49, no. 3–4, pp. 407–423 (2000).

[13] Szeląg A., *Rail track as a lossy transmission line. Part II: New method of measurements-simulation and in situ measurements*, Archives of Electrical Engineering, vol. 49, no. 3–4, pp. 425–453 (2000).

[14] Ivanek L., Mostyn V., Schee K., Grun J., *The Sensitivity of the Input Impedance Parameters of Track Circuits to Changes in the Parameters of the Track*, Advances in Electrical and Electronic Engineering, vol. 15, no. 1, pp. 77–83 (2017).

[15] Journey M.P., Steel O.J., Forte B.K., *Modelamiento electromagnético de los sistemas eléctricos ferroviarios para estudiar su compatibilidad*, Revista Digital Lámpsakos, no. 3, pp. 42–47 (2010).

[16] Guglielmino E., *Determinación de parámetros electromagnéticos de vías férreas*, Ingenierías, vol. 6, no. 19, p. 39 (2003).

[17] Bongiorno J., Mariscotti A., *Variability of pantograph impedance curves in DC traction systems and comparison with experimental results*, Przegląd Elektrotechniczny, vol. 90, no. 6, pp. 178–183 (2014).

[18] D'Addio G., Fracchia M., Mariscotti A., Pozzobon P., *Sensitivity analysis of railway line impedance to variations of electrical and geometrical parameters*, Proceedings of the World Congress on Railway Research WCRR 99, Tokyo (1999).

[19] CCITT Directive, *Calculating induced voltages and currents in practical cases*, Geneva, Switzerland, vol. II (1989).

[20] Ramo S., Winnery J.R., van Duzer T., *Fields and waves in communication electronics*, New York, J. Wiley & Sons, pp. 291–297 (1965).

[21] Illias H.A., Abu Bakar A.H, Mokhlis H., Halim S.A., *Calculation of inductance and capacitance in power system transmission lines using finite element analysis method*, Przegląd Elektrotechniczny, vol. 88, no. 10, pp. 278–283 (2012).

[22] Di Rienzo L., Zhang Z., Pignari S.A., *Boundary-element computation of per-unit-length series parameters of railway lines*, IEEE Trans. on Electromagnetic Compatibility, vol. 51, no. 3, pp. 825–832 (2009).

[23] D'Amore M., Sarto M.S., *Simulation models of a dissipative transmission line above a lossy ground for a wide-frequency range – Part II: Multi conductor configuration*, IEEE Trans. on Electromagnetic Compatibility, vol. 38, no. 2, pp. 139–149 (1996).

[24] Robinson D.A., *Measurement of the solid dielectric permittivity of clay minerals and granular samples using a time domain reflectometry immersion method*, Vadose Zone Journal, vol. 3, pp. 705–713 (2004), www.vadosezonejournal.org, accessed April 2019.

[25] Martinez A., Byrnes A.P., *Modelling dielectric-constant values of geologic materials: an aid to ground-penetrating radar data collection and interpretation*, Current Research in Earth Sciences, Bulletin 247, part 1 (http://www.kgs.ukans.edu/Current/2001/martinez/martinez1.html) (2001).

[26] Olhoeft G.R., *Electrical properties of rocks* in *Physical Properties of Rocks and Minerals*, Hemisphere Publishing Corporation, New York, pp. 257–329 (1989).

[27] Edwards R.J., *Skin Depth in the Ground vs. Frequency for Given Soil Characteristics*, March 18 (1999), www.smeter.net, accessed April 2019.

[28] Scott J.H., Carrol R.D., Cunningham D.R., *Dielectric constant and electrical conductivity measurements of moist rock: a new laboratory method*, Journal of Geophysical Research, vol. 27, no. 20 (1967).

[29] Tabbagh A., Hesse A., Grard R., *Determination of electrical properties of the ground at shallow depth with an electrostatic quadrupole: field trials on archaeological sites*, Geophysical Prospection, vol. 41, pp. 579–597 (1993).

[30] Robinson D.A. *et al.*, *Considerations for improving the accuracy of permittivity measurement using time domain reflectometry: air-water calibration, effects of cable length*, Journal of Soil Science Society of America, vol. 67, pp. 62-67 (2003).

[31] Longley-Rice soil characteristics (2003), www.softwright.com, accessed April 2019.

[32] Mariscotti A., Pozzobon P., *Experimental results on low rail-to-rail conductance values*, IEEE Trans. on Vehicular Technology, vol. 54, no. 3, pp. 1219–1222 (2005).

[33] Sverko E.R., *Ground measuring techniques: electrode resistance to remote earth & soil resistivity*, Feb. 11 (1999), www.erico.com, accessed April 2019.

[34] *Table of resistivity values*, http://hyperphysics.phy-astr.gsu.edu/hbase/Tables/rstiv.html, accessed April 2019.

[35] IEEE Std. 81, *IEEE Guide for measuring earth resistivity, ground impedance and earth surface potentials of a ground system* (1983).

[36] ANSOFT Maxwell, https://www.ansys.com/academic/free-student-products, accessed April 2019.